Optimization and Comparison of Permanent Magnet Synchronous Motors with Mechanically and Magnetically Coupled Magnetic Gears at Different Gear Ratios for Helicopter Applications

Shima Hasanpour
Dept. of Elec. & Comp. Eng
Texas A&M University
College Station, TX, USA
shimahasanpour@tamu.edu

Matthew C. Gardner
Dept. of Elec. & Comp. Eng
University of Texas at Dallas
Richardson, TX, USA
matthew.gardner@utdallas.edu

Matthew Johnson
FluxWorks LLC
College Station, TX, USA
matt@fluxworksllc.com

Hamid A. Toliyat
Dept. of Elec. & Comp. Eng
Texas A&M University
College Station, TX, USA
toliyat@tamu.edu

***Abstract*—Permanent magnet synchronous motors (PMSMs) are suggested for applications with high torque density, reliability, and efficiency requirements. Integrating PMSMs with magnetic gears (MGs), magnetically geared motors (MGMs), can potentially increase the torque density and reliability of the system. There are two common radial flux inner stator MGM topologies, mechanically coupled and magnetically integrated MGMs. This study independently optimized PMSMs, mechanically coupled MGMs, and magnetically integrated MGMs using 2D finite element analysis (FEA) with a genetic algorithm (GA) to maximize the specific torque (ST), the maximum achievable torque divided by the active mass, for a thorough comparison. Multiple gear ratios and slot/pole-pair (SPP) combinations were considered. As expected the MGMs outperform the PMSMs in terms of ST and magnet usage. Additionally, the analysis shows a reduction in the performance of magnetically integrated MGMs at higher gear ratios as the pole pairs of the MG are dependent on the selected SPP and may not represent the optimal MG at a certain gear ratio. Nonetheless, at lower gear ratios, magnetically integrated MGMs achieve higher ST by utilizing a thin back-iron on the high-speed rotor (HSR). The 3D simulations demonstrate that the optimal MGMs experience more substantial torque drops compared to direct-drive motors, especially at higher gear ratios. These torque reductions are a result of end effects and axially escaping flux, inherent features of MGs. MGMs manage to achieve comparable efficiencies to direct-drive motors at lower gear ratios while offering the advantage of lower mass and volume.**

Keywords*——*Magnetic gears, direct drive, permanent magnet synchronous machine, optimization, finite element analysis (FEA), genetic algorithm (GA), torque density.

I. Introduction

Permanent magnet synchronous machines (PMSMs) are widely used in various industries including electric vehicles [1], aircrafts including electric helicopter [2]-[3], and wind turbines [4]. PMSMs offer precise speed and position control, low noise and vibration, and long lifespan. Additionally, the key advantages of PMSMs are their high efficiency and power density [1]-[5], which makes them an ideal choice for applications where space and weight are critical factors. Further improvement of the specific torque (ST), the maximum achievable torque divided by the active mass, of PMSMs would make them more suitable for applications that require high acceleration or maneuverability. In robotics and industrial automation, higher torque density can enable more precise and agile movements, which can improve productivity and safety. However, the ST of PMSMs at a fixed shaft speed is limited by their current density and permanent magnet (PM) volume. Increasing the current density increases the ohmic losses, whereas increasing PM volume increases mass and cost.

The utilization of geared machines instead of direct drive machines has been suggested for specific applications, such as wind turbines [6]. By incorporating a gearbox to transmit power to the high-torque shaft of the system, it becomes possible to attain the target torque with a lighter weight and lower torque generator. Employing gears with lower torque rating machines enables reduction of the overall system weight and size. However, it is important to address potential challenges arising from the gearbox performance, which can impact system reliability, overall efficiency, and noise levels.

Magnetic gears (MGs) are interesting alternatives to conventional mechanical gears, facilitating power transmission between a low-speed, high-torque shaft and a high-speed, low-torque shaft through modulated magnetic fields instead of mechanical teeth interlock. Consequently, MGs potentially

This work was supported in part by the U.S. Army Research Laboratory and was accomplished under Cooperative Agreement Number W911NF-18-2-0289. The views and conclusions contained in this document are those of the authors and should not be interpreted as representing the official policies, either expressed or implied, of the Army Research Laboratory or the U.S. Government. The U.S. Government is authorized to reproduce and distribute reprints for Government purposes notwithstanding any copyright notation herein.

require less maintenance, operate at lower acoustic noise, and provide higher reliability in the system level that could address some of the challenges in applications like traction [7], propulsion [8], electric vertical take-off and landing aircraft [9], and wind [10] and wave energy [11]. Among various MG topologies, the radial flux coaxial magnetic gear stands out as the most extensively studied, featuring different PM configurations, such as surface permanent magnet [12]-[16], flux focusing [17]-[18], Halbach array [19]-[22], and reluctance [23]-[24].

The integration of coaxial surface permanent magnet MGs and PMSMs has gained significant attention in recent years due to its potential to provide a compact, torque dense, and efficient solution for power transmission [25]-[33]. MGs employ the interaction between magnetic fields to transfer torque, making them an ideal complement to electric motors. The combination of the two technologies offers several advantages, including high torque density, low noise, and maintenance-free operation.

Electric helicopters present a promising and impactful application for magnetically geared motors (MGMs), offering significant advantages over conventional helicopters in the context of urban transportation. Traditional helicopters rely on mechanical gears that are prone to wear and tear, resulting in higher maintenance costs and increased downtimes, and may overheat in loss-of-lubrication events. In contrast, MGMs leverage magnetic gears, ensuring non-contact operation and eliminating the need for lubrication. This feature enhances the system's reliability, which is critical for urban transportation. Moreover, MGMs demonstrate the capability to deliver the target torque at a lower weight and volume. This reduction in mass increases the payload of electric helicopters, making MGMs a more suitable powertrain solution for urban transportation applications. To contribute to the advancement of electric helicopters as a feasible urban transportation option, this paper focuses on optimizing MGMs to deliver the 400 Nm torque, which is in the same range achieved by an existing helicopter engine, the Rolls-Royce 250-C20 engine used in 206B Jet Ranger II [34].

The existing literature studied various MGM topologies, including an inner stator MGM [25]-[27] or an outer stator MGM [28]-[29]. Additionally, inner stator MGMs could be mechanically coupled or magnetically integrated. Fig. 1 shows the cross-sections of a direct drive motor, a mechanically coupled MGM, and a magnetically integrated MGM. As shown in Fig. 1(c), in a magnetically integrated MGM, the motor and the MG's high speed rotor (HSR) have the same number of poles with only a thin back iron, which is primarily for mechanical and assembly purposes. However, in a mechanically coupled MGM, the motor may have a different number of poles than the MG's HSR, and the back iron is thicker to magnetically decouple the motor and MG fluxes.

Most of the existing literature on the performance of MGMs are limited to the following two conditions, which are inadequate for a thorough performance evaluation of MGMs.

- Optimization and analysis of only magnetically integrated MGM over different dimensional parameters and/or slot/pole-pair (SPP) combinations, [26]-[29]. Refs. [32] and [33] expanded the optimization to multiple gear ratios.
- Comparison of non-optimized mechanically coupled with magnetically integrated MGMs [31]. Ref. [31] compares an optimized motor with an optimized magnetically integrated MGM but at only at a single gear ratio.

Therefore, this paper presents the results from an independent optimization of three topologies, a direct drive motor, an inner

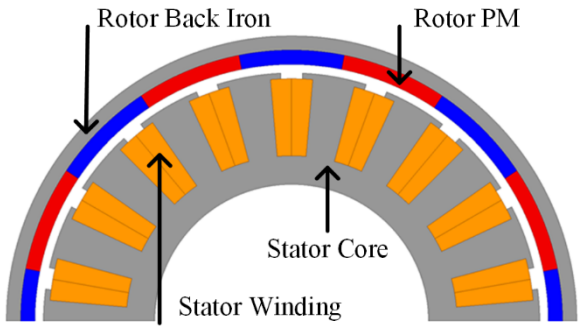

(a)

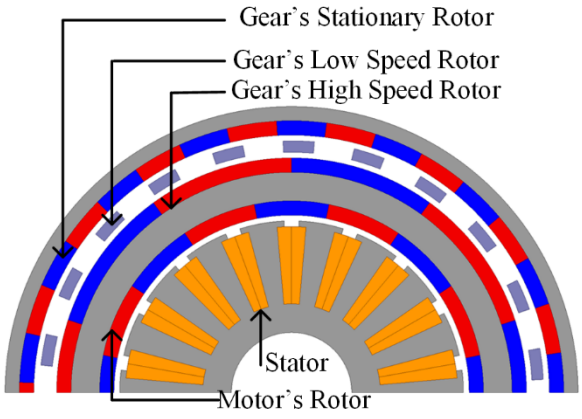

(b)

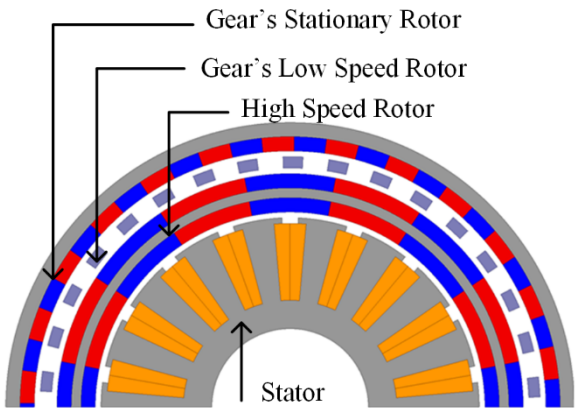

(c)

Fig. 1: Cross-sections of (a) direct drive motor, (b) mechanically coupled MGM, and (c) magnetically integrated MGM.

stator mechanically coupled MGM, and an inner stator magnetically integrated MGM, using a 2D finite element analysis (FEA) and a genetic algorithm (GA) across multiple gear ratios, SPP combinations, and a broad range of design parameters. Then, the 2D transient FEA and 3D FEA were used to evaluate the efficiency and end effects of the optimal designs at target torque of 400 Nm, which is about the take-off torque in the Bell 206 Jet Ranger helicopters. This will be the first paper to compare independently optimized inner stator direct drive motor, mechanically coupled, and magnetically integrated MGMs at multiple gear ratios and SPP combinations.

II. Design Study Methodology

Each topology show in Fig. 1 was independently optimized for ST using a GA across six different SPP combinations for the motor and a range of gear ratios for the MGMs. The GA employed 2D FEA to optimize each topology, evaluating 100 generations of approximately 1000 individual designs each, with the primary objective of maximizing ST. Table I provides a summary of the extensive range of values considered for the design parameters. In addition to the parameters listed in Table I, the optimization also took into account three grades of NdFeB, N52M, N50H, and N48SH for the PMs. The ferromagnetic components including stator core, teeth, back irons, and modulators used 29-gauge M19 silicon steel.

The tooth fill factor is defined as the ratio of the angular width of a tooth to the combined angular width of a tooth and a slot. A high tooth fill factor value implies that the design allocates a larger area to the tooth while the available area for the windings is reduced. Therefore, the GA converged toward designs with lower tooth fill factor to provide more area for the windings, resulting in higher amp-turns and, consequently, higher torques. Another important parameter is copper fill factor, which represents the fraction of the slot area that is filled with copper windings. The slot opening factor is determined as the ratio of the slot opening arc length (between adjacent tooth tips) to the arc length of the full slot's outer edge.

To avoid designs with large torque ripples, integer gear ratio designs are excluded [35]-[36]; hence, the PM pole pair counts on the stationary rotor of the MG are given by (1). The number of modulators on the low-speed high-torque rotor is then derived using (2). So (3) provides the gear ratio in the MGMs, where the ratio of the high-speed rotor's speed is divided by the low-speed rotor's rotational speed, with the outer rotor being held fixed.

$$P_{Stationary} = \begin{cases} G_{Int}P_{HS} + 1 & \text{for } (G_{Int}+1)P_{HS} \text{ odd} \\ G_{Int}P_{HS} + 2 & \text{for } (G_{Int}+1)P_{HS} \text{ even} \end{cases} \quad (1)$$

$$Q_{Mods} = P_{HS} + P_{Stationary} \quad (2)$$

$$Gear\ Ratio = \frac{\omega_{HS}}{\omega_{Mods}} = \frac{Q_{Mods}}{P_{HS}} \quad (3)$$

The range of gear ratios considered for the mechanically coupled MGM differs from that of the magnetically integrated MGMs. It was observed that the performance of the magnetically integrated MGMs began to decline beyond the maximum gear ratio reported here, which will be discussed in the subsequent section.

TABLE I. GA Parameter Value Ranges

Parameter	Values
Outer radius (mm)	100
Stator phases	3
Stator back iron thickness (mm)	1 – 20
Stator slot thickness (mm)	1 – 30
Stator tooth tips thickness (mm)	1 – 10
Air gap thickness (mm)	1
PM thickness (mm)	1 - 20
Rotors back iron thickness (mm)	1 – 20
Modulators thickness (mm)	2 – 15
Tooth fill factor	0.1 – 0.9
Copper fill factor	0.4
Slot opening factor	0.05 - 1
PM tangential fill factor	0.1 - 1
Modulator tangential fill factor	0.05 – 0.95
Integer part of the gear ratio (G_{Int}) Mechanically Coupled MGM Magnetically Integrated MGM	 4, 6, 8, …, 24 4, 6, 8, …, 14
High-speed rotor PM pole pairs in Mechanically Coupled MGM (P_{HS})	3, 4, …, 15
Current density rms (A/mm^2)	3.5

In mechanically coupled MGMs, the optimization objectives for both the motor and MG went beyond maximizing ST, as these two topologies were simulated and optimized independently. In addition to optimizing ST, the MG aimed to maximize the inner radius, while the motor focused on minimizing the outer radius. Subsequently, a script was employed to discover the optimized motors that can be accommodated within the MG at any gear ratio and for all SPP combinations.

The considered SPP combinations are listed in Table II (also the legend for later figures), which indicate high-performance SPP combinations for tooth-wound motors with fundamental winding factors over 0.9.

III. Result

The results of the GA optimization studies are summarized in Fig. 2. The plots present the maximum achievable ST within the parameter ranges allowed in the GA at multiple gear ratios for different SPP combinations, distinguished by the colors. The points at the gear ratio equal to 0 represent the performance of the optimized direct drive motor without any magnetic gear. Fig. 2 illustrates the limited capability of the direct drive motor to

TABLE II. EVALUATED SPP COMBINATIONS

Slot/Pole Pair	Mechanically Coupled MGM	Magnetically Integrated MGM
12/7		
24/10		
27/12		
24/13		
24/14		
36/15		

achieve higher STs within the same outer radius as the MGMs for the 6 studied SPP combinations. Comparing Fig. 2(a) and 2(b) shows that at lower gear ratios, magnetically integrated MGMs slightly outperform mechanically coupled MGMs, which is due to the use of a thin back iron on the high-speed rotor in magnetically geared MGMs that creates additional space for the inner stator and consequently result in increased torque. On the other hand, as the gear ratio increases, the ST of magnetically integrated MGM starts to decline. This drop in performance is a consequence of the motor and MG's HSR being constrained to have the same number of pole pairs. On the other hand, in mechanically coupled MGMs, the MG's pole count optimization is independent of the motor's SPP combination.

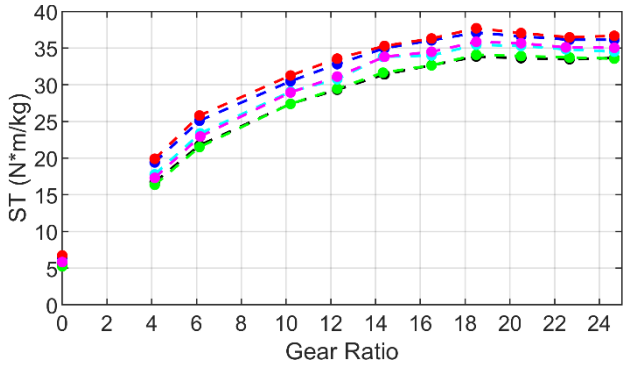

(a)

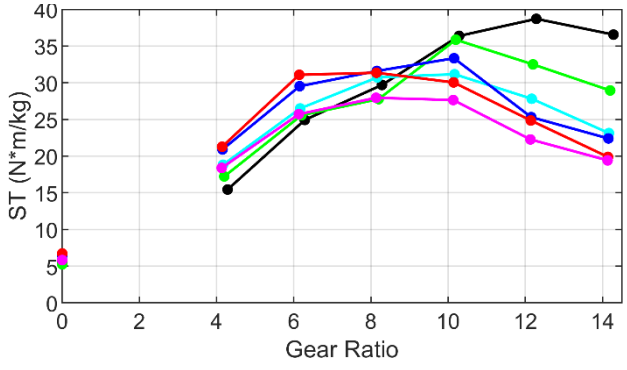

(b)

Fig. 2: Impact of gear ratio on the maximum achievable ST of (a) mechanically coupled MGMs and (b) magnetically integrated MGMs for the different SPP combinations.

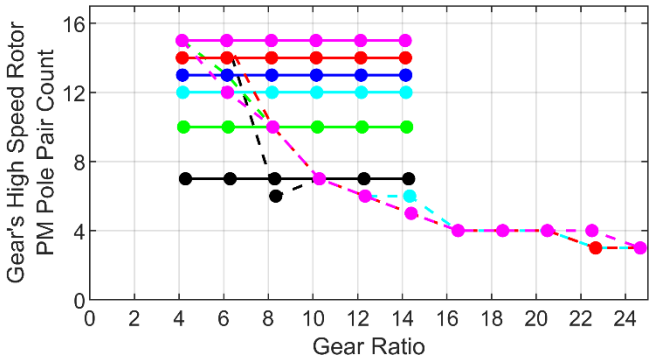

(a)

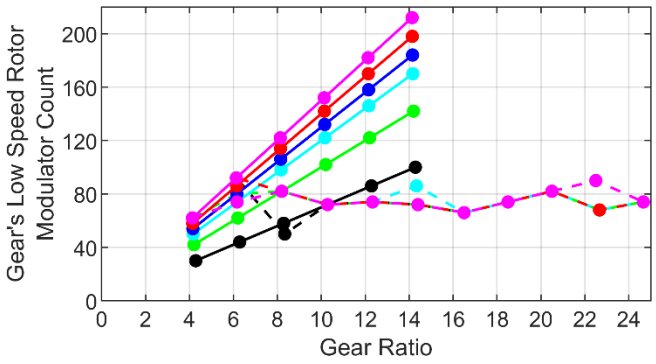

(b)

Fig. 3: Corresponding (a) gear's high speed rotor PM pole pair and (b) gear's low speed rotor modulator counts for the maximum ST designs.

Therefore, as shown in Fig. 3 (a), the optimal PM pole pairs of MG's HSR decrease at higher gear ratios in optimal mechanically coupled MGMs, while they stay constant in optimal magnetically integrated MGMs. Fig. 3(b) shows the modulator counts on the low speed rotor of MGs. Magnetically integrated MGMs include significantly higher piece counts on their rotors at higher gear ratios, which corresponds to higher leakage flux due to the shorter arc length of the PM pieces and modulators. This effect is also reflected in Fig. 2(b), where this leakage flux reduces the ST at higher gear ratios.

Figs. 4 focuses on a single SPP combination, 24/10, to simplify and magnify the difference in the performance of mechanically coupled and magnetically integrated MGMs. Fig. 4 shows the overall required PM mass for each topology to achieve the torque of 400 Nm. A significant advantage of the MGMs is the reduction in the PM mass, where the direct drive motor employs about 3 times as much PM mass to attain the same torque as the MGMs [37]-[38]. This reduction in PM mass directly translates to a material cost reduction as the PMs are the most expensive components compared to the copper and steel. It should be emphasized that MGMs require significantly higher PM piece counts, but this does not result in an overall increase in the weight of the PMs. On the contrary, the required PM mass for MGMs is notably lower than that of the direct drive motor, indicating that the required stack length of the PMs in MGMs is

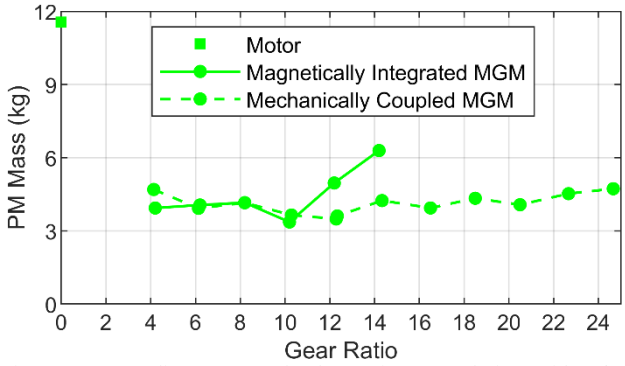

Fig. 4: Corresponding PM mass for the maximum ST designs with 24/10 SPP combination.

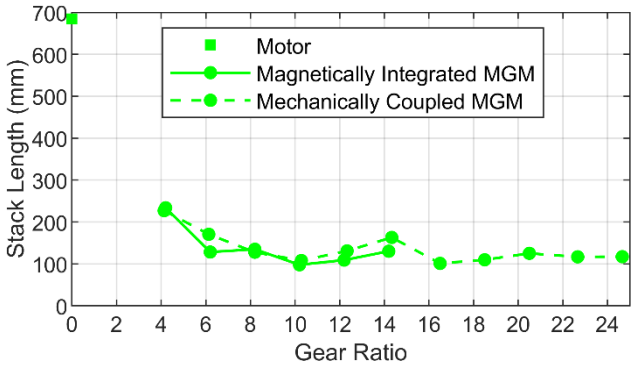

Fig. 5: Corresponding stack length for the maximum ST designs with 24/10 SPP combination.

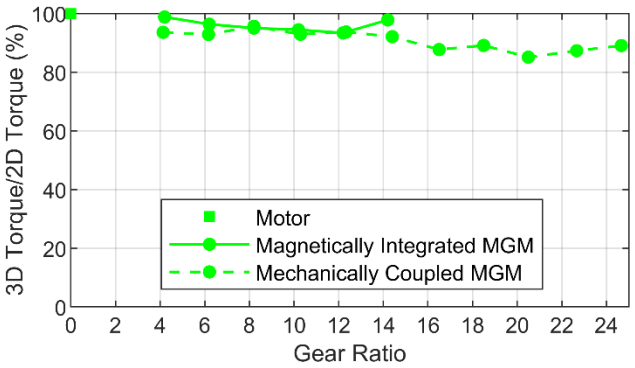

Fig. 6: Corresponding ratio of 3D simulation torque to 2D simulation torque for the maximum ST designs with 24/10 SPP combination at stack lengths shown in Fig. 5.

much shorter than in direct drive motors.

Fig. 5 shows the required stack length of the three topologies with SPP combination 24/10 in order to achieve the 400 Nm target torque, determined using 2D FEA simulations. The direct drive motor is significantly longer compared to the MGMs, whereas the MGMs take advantage of employing torque-dense MGs, resulting in a lower required stack length. On the other hand, it is important to note that the reduction in the required stack length may potentially lead to a decrease in the achievable torque in 3D simulations due to higher axial leakage and escaping flux.

All three topologies, direct drive motor, magnetically integrated and mechanically coupled MGMs, were simulated at the required stack lengths indicated in Fig. 5 using 3D FEA simulations. Fig. 6 shows the corresponding ratio of 3D torque over 2D torque at different gear ratios. As expected, the direct drive motors experience less 3D end effects compared to the MGMs, because there are two opposing sets of PMs facing each other in MGMs that produce axially escaping flux and cause torque reduction in 3D analysis.

As the gear ratio increases, the optimal PM pole pair count on the MG's HSR in mechanically coupled MGMs reduces to

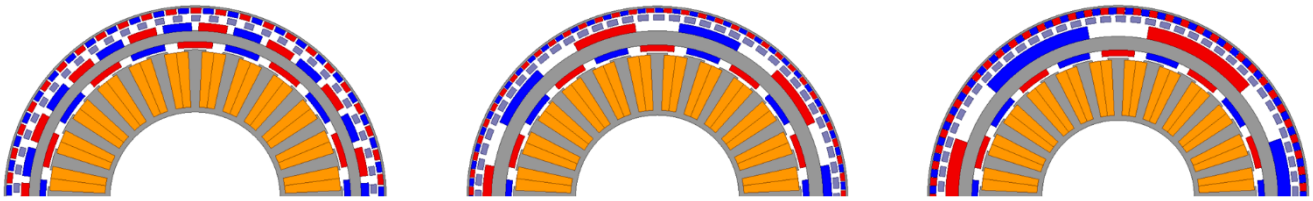

(a) (b) (c)

Fig. 7: Cross-sectional portions of mechanically coupled MGMs with 24/10 SPP combination and integer part of gear ratio (a) 4, (b) 14, and (c) 24 that achieve the maximum ST.

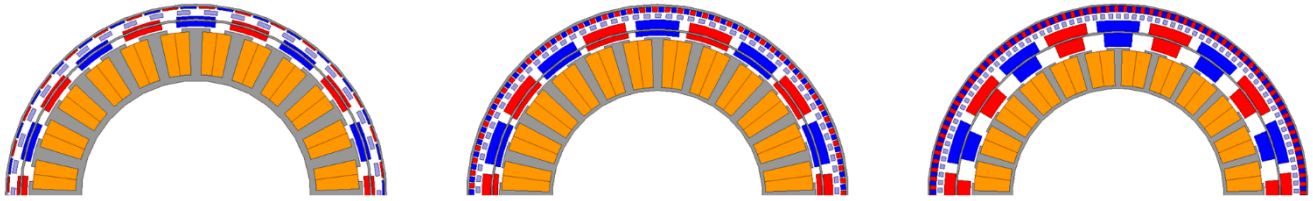

(a) (b) (c)

Fig. 8: Cross-sectional portions of magnetically integrated MGMs with 24/10 SPP combination and integer part of gear ratio (a) 4, (b) 10, and (c) 14 that achieve the maximum ST.

mitigate high piece counts involving modulators and stationary rotor PMs. Consequently, the arc length of PMs on MG's HSR become very long, as shown in cross sections of Fig. 7. On the other hand, the arc lengths of the PMs on the outer stationary rotor decrease to accommodate all the PM pieces. This causes an increase in leakage flux at higher gear ratios, intensifying the impact of end effects.

Fig. 8 shows the corresponding cross-sections of optimal magnetically integrated MGMs. Comparing Figs. 8 and 7 shows the consequences of dependent optimization of MG and motor in the magnetically integrated MGM as the PM pole pair on the HSR is fixed at the pole count determined by SPP combination of the motor. However, since the back-iron on the HSR is thin and only for manufacturing constraints, there is more space available for the stator

The loss analyses of the direct drive motor, mechanically coupled, and magnetically integrated MGMs are presented in Fig. 9 and Fig. 10, respectively; focusing on the electromagnetic efficiency, per unit (pu) AC loss from core losses in the steel and eddy currents in the magnets, and pu DC copper loss for the optimal ST designs, operating at a target torque of 400 Nm and an output speed of 250 rpm. The figures display noise because the topologies are primarily optimized for the ST rather than efficiency. Despite the noise, the figures still clearly reveal the trends in losses as the gear ratio changes. The pu loss denotes the losses relative to the output power, which remains constant at 10.47 kW for all designs.

A comparison between Figs. 9 and 10 reveals that the efficiency of the MGMs at lower gear ratios are comparable to that of direct drive motors, while simultaneously achieving the target power with lower mass, as shown in Fig. 2. Nevertheless, the efficiency of the MGMs at higher gear ratios will experience a substantial decline compared to that of the direct drive motor, even when targeting the same power output. This drop in performance of the MGMs is a result of operating at higher speeds, where the high-speed rotor rotates at a speed equal to the product of the gear ratio and the output speed (250 rpm), than the direct-drive motor, which is fixed at 250 rpm, leading to increased frequency and subsequently higher AC losses, as discussed in [39].

The decrease in copper losses with increasing gear ratio is attributed to the motor's deliverable torque being reduced by the gear ratio, consequently requiring less winding volume and leading to lower copper losses, as depicted in Figs. 9(c) and 10(c). The direct-drive motor has significantly higher DC copper losses as it requires about much more active material mass (including copper) to deliver the target torque based on Fig. 2. Additionally, the AC losses include the core losses, which increase as the gear ratio increases due to the increase in the electromagnetic frequency as illustrated in Fig. 9(b) and 10(b).

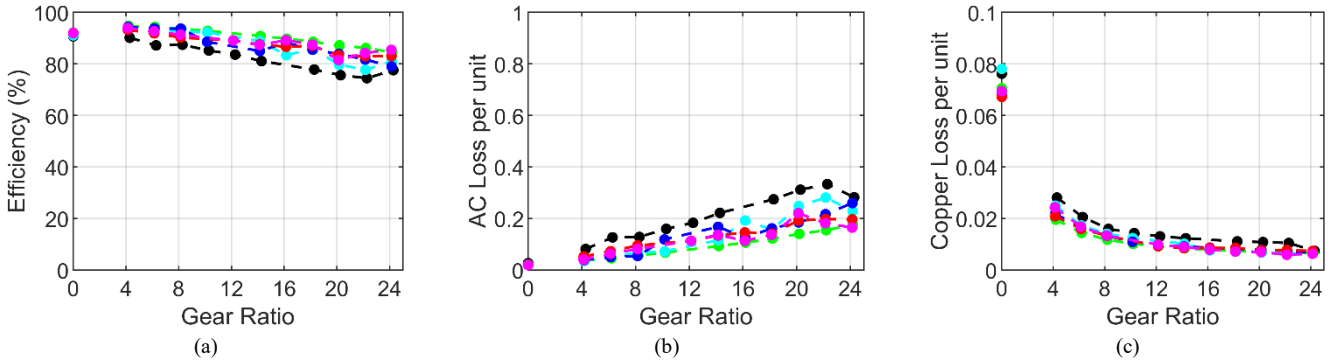

Fig. 9: Corresponding (a) efficiency, (b) AC losses, and (c) DC copper losses for the maximum ST Mechanically Coupled MGM designs show in Fig. 2(a).

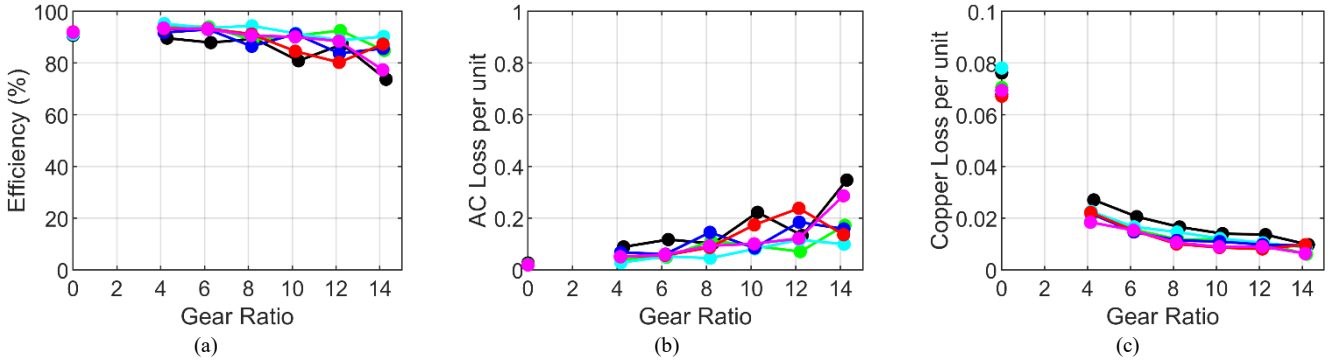

Fig. 10: Corresponding (a) efficiency, (b) AC losses, and (c) DC copper losses for the maximum ST Magnetically Integrated MGM designs show in Fig. 2(b).

IV. Conclusion

This paper compares the independently optimized direct drive PMSMs, mechanically coupled MGMs, and magnetically integrated MGMs. A GA and 2D static FEA were used to parametrically optimize each topology for maximum ST across multiple gear ratios and SPP combinations. The optimal 2D designs were further investigated using 3D static FEA and 2D transient FEA to evaluate the torque drop caused by the end-effects and the efficiency, respectively. Following are the conclusions from the simulation results within the evaluated design space:

- The maximum achievable ST for the direct drive motors is limited and much lower than that of MGMs.
- Magnetically integrated MGMs achieve slightly higher STs than mechanically coupled MGMs because the HSR's back-iron is thin and there is more space available for the stators.
- The STs of magnetically integrated MGMs start to drop at lower gear ratios than mechanically coupled MGMs since the PM pole pair counts on the magnetically integrated gear's HSR are determined by the SPP combination of the motor, causing the MG design to significantly exceed the optimal pole pair combination at higher gear ratios and, consequently, suffer from excessive leakage flux.
- Both evaluated types of MGMs require significantly less volume, active mass, and PM mass than direct drive motors to achieve the same torque.
- MGMs suffer more from the 3D end effects as there are two sets of opposing PMs causing axial escaping flux.
- The torque drop in 3D simulations of mechanically coupled MGMs increase with the gear ratio because the MG tends to reduce the optimal PM pole counts on the HSR and increase the PM pole counts on the outer rotor, which results in a design with PM pole counts that are farther from the optimal values.
- The efficiency of MGMs at lower gear ratios are close to that of the direct drive motors, while their mass is significantly lower than that of the direct drive motors.
- MGMs' efficiency decrease as the gear ratio increases since the rotational speed increases and results in higher AC losses.
- MGMs' DC copper losses decrease at higher gear ratio since the motor's torque reduces so the motor gets smaller.

Acknowledgment

Portion of this research were conducted with the advanced computing resources provided by Texas A&M Performance Research Computing. The authors would like to thank ANSYS for their support of the EMPE lab through the provision of FEA software.

References

[1] Q. Chen, G. Liu, W. Gong and W. Zhao, "A new fault-tolerant permanent-magnet machine for electric vehicle applications," *IEEE Trans. Magn*., vol. 47, no. 10, pp. 4183-4186, Oct. 2011.

[2] M. Villani, M. Tursini, G. Fabri and L. Castellini, "High reliability permanent magnet brushless motor drive for aircraft application," *IEEE Trans. Ind. Electron*., vol. 59, no. 5, pp. 2073-2081, May 2012.

[3] I. Bolvashenkov, J. Kammermann, S. Willerich, and H.-G. Herzog, "Comparative study for the optimal choice of electric traction motors for a helicopter drive train," in *Proc. .Sustainable Development of Energy, Water and Environment Systems*, Sept. 2015.

[4] K. -J. Ko, S. -M. Jang, J. -H. Park, H. -W. Cho and D. -J. You, "Electromagnetic performance analysis of wind power generator with outer permanent magnet rotor based on turbine characteristics variation over nominal wind speed," *IEEE Trans. Magn*., vol. 47, no. 10, pp. 3292-3295, Oct. 2011.

[5] S. Hasanpour, S. Sheshaprasad, M. C. Gardner, M. Johnson, B. Praslicka and H. A. Toliyat, "Design and Control of a Fault Tolerant Permanent Magnet Motor with Independently Optimized Phase and Pole Counts," in *Proc. Symp. Diagnostics Elect. Mach., Power Electron. Drives*, 2021, pp. 58-64.

[6] H. Polinder, F. F. A. van der Pijl, G. . -J. de Vilder, and P. J. Tavner, "Comparison of direct-drive and geared generator concepts for wind turbines," *IEEE Trans. Energy Conv*., vol. 21, no. 3, pp. 725-733, Sept. 2006.

[7] T. Frandsen, L. Mathe, N. Berg, R. Holm, T. Matzen, P. Rasmussen, and K. Jensen, "Motor integrated permanent magnet gear in a battery electrical vehicle," *IEEE Trans. Ind. Appl*., vol. 51, no. 2, pp. 1516–1525, Mar./Apr. 2015.

[8] L. MacNeil, B. Claus, and R. Bachmayer, "Design and evaluation of a magnetically-geared underwater propulsion system for autonomous underwater and surface craft," in *Proc. Int. Conf. IEEE Oceans*, 2014, pp. 1-8.

[9] T. F. Tallerico, Z. A. Cameron and J. J. Scheidler, "Design of a magnetic gear for nasa's vertical lift quadrotor concept vehicle," in *Proc. AIAA/IEEE Elect. Aircr. Technol. Symp*, 2019, pp. 1-21.

[10] N. Frank and H. Toliyat, "Gearing ratios of a magnetic gear for wind turbines," in *Proc. IEEE Int. Elect. Mach. Drives Conf*., 2009, pp. 1224-1230.

[11] K. K. Uppalapati, J. Z. Bird, D. Jia, J. Garner, and A. Zhou, "Performance of a magnetic gear using ferrite magnets for low speed ocean power generation," in *Proc. IEEE Energy Convers. Congr. Expo*., 2012, pp. 3348–3355.

[12] J. Scheidler, V. Asnani, and T. Tallerico, "NASA's magnetic gearing research for electrified aircraft propulsion," in *Proc. AIAA/IEEE Elect. Aircr. Technol. Symp.,* Jul. 2018, pp. 1–12.

[13] K. Atallah and D. Howe, "A novel high-performance magnetic gear," *IEEE Trans. Magn*., vol. 37, no. 4, pp. 2844–2846, Jul. 2001.

[14] P. O. Rasmussen, T. O. Andersen, F. T. Jorgensen, and O. Nielsen, "Development of a high-performance magnetic gear," *IEEE Trans. Ind. Appl.*, vol. 41, no. 3, pp. 764–770, May/Jun. 2005.

[15] P. M. Tlali, R.-J. Wang, and S. Gerber, "Magnetic gear technologies: A review," in *Proc. Int. Conf. Electr. Mach.*, Sep. 2014, pp. 544–550.

[16] Y. Wang, M. Filippini, N. Bianchi, and P. Alotto, "A review on magnetic gears: Topologies, computational models, and design aspects," *IEEE Trans. Ind. Appl.*, vol. 55, no. 5, pp. 4557–4566, Sep./Oct. 2019.

[17] K. Li, S. Modaresahmadi, W. B. Williams, J. Z. Bird, J. D. Wright, and D. Barnett, "Electromagnetic analysis and experimental testing of a flux focusing wind turbine magnetic gearbox," *IEEE Trans. Energy Conv*., vol. 34, no. 3, pp. 1512–1521, Sep. 2019.

[18] S. Sheshaprasad, M. Johnson, H. A. Toliyat, "Design Optimization of Radial Flux-Focusing Coaxial Magnetic Gears and Comparison with Conventional Surface Permanent Magnet and Halbach Topologies", in *Proc. IEEE Energy Convers. Congr. Expo*., 2023.

[19] L. Jian and K. T. Chau, "A coaxial magnetic gear with Halbach permanent-magnet arrays," *IEEE Trans. Energy Conv*., vol. 25, no. 2, pp. 319–328, Jun. 2010.

[20] L. Jian, K. T. Chau, Y. Gong, J. Z. Jiang, C. Yu, and W. Li, “Comparison of coaxial magnetic gears with different topologies,” *IEEE Trans. Magn*., vol. 45, no. 10, pp. 4526–4529, Oct. 2009.

[21] M. Johnson, M. C. Gardner, and H. A. Toliyat, “Analysis of axial field magnetic gears with Halbach arrays,” in *Proc. IEEE Int. Electr. Mach. Drives Conf*., May 2015, pp. 108–114.

[22] H. Huang, R. Qu, and J. Bird, “Performance of Halbach cycloidal magnetic gears with respect to torque density and gear ratio,” in *Proc. IEEE Int. Electr. Mach. Drives Conf.*, May 2019, pp. 1977–1984.

[23] S. Hasanpour, M. C. Gardner, M. Johnson, and H. A. Toliyat, “Comparison of reluctance and surface permanent magnet coaxial magnetic gears,” in *Proc. IEEE Energy Convers. Congr. Expo*., Oct. 2020, pp. 307–314.

[24] K. Aiso, K. Akatsu, and Y. Aoyama, “A novel reluctance magnetic gear for high-speed motor,” *IEEE Trans. Ind. Appl*., vol. 55, no. 3, pp. 2690–2699, May/Jun. 2019.

[25] K. Ito and K. Nakamura, "Investigation of magnetic interaction of IPM-type magnetic-geared motor," *IEEE Trans. Magn*., vol. 57, no. 2, pp. 1-5, Feb. 2021.

[26] A. B. Kjaer, S. Korsgaard, S. S. Nielsen, L. Demsa and P. O. Rasmussen, "Design, fabrication, test, and benchmark of a magnetically geared permanent magnet generator for wind power generation," *IEEE Trans. Energy Conv*., vol. 35, no. 1, pp. 24-32, March 2020.

[27] S. Gerber and R. -J. Wang, "Design and evaluation of a magnetically geared PM machine," *IEEE Trans. Magn*., vol. 51, no. 8, pp. 1-10, Aug. 2015.

[28] P. M. Tlali, S. Gerber and R. -J. Wang, "Optimal design of an outer-stator magnetically geared permanent magnet machine," *IEEE Trans. Magn*., vol. 52, no. 2, pp. 1-10, Feb. 2016.

[29] H. Huang, D. Li, W. Kong and R. Qu, "Torque performance of pseudo direct-drive machine with halbach consequent pole," in *Proc. IEEE Energy Convers. Congr. Expo.,* 2018, pp. 3286-3293.

[30] S. Gerber and R. -J. Wang, "Torque capability comparison of two magnetically geared PM machine topologies," in Proc. *IEEE Int. Conf. on Ind. Technol.,* 2013, pp. 1915-1920.

[31] W. Zhao, J. Liu, J. Ji, G. Liu and Z. Ling, "Comparison of coaxial magnetic gears with and without magnetic conducting ring," *IEEE Trans. Appl. Supercond*., vol. 26, no. 4, pp. 1-5, June 2016.

[32] R. S. Dragan, R. E. Clark, E. K. Hussain, K. Atallah and M. Odavic, "Magnetically geared pseudo direct drive for safety critical applications," in *Proc. IEEE Int. Elec. Mach. Drives Conf*.,2017, pp. 1-8.

[33] T. F. Tallerico, Z. A. Cameron, J. J. Scheidler and H. Hasseeb, "Outer Stator MagneticallyGeared Motors for Electrified Urban Air Mobility Vehicles," in *Proc. AIAA/IEEE Elect. Aircraft Technol. Symp*., 2020, pp. 1-25.

[34] https://aircraft-database.com/database/engine-models/250-c20b

[35] M. Johnson, M. C. Gardner, and H. A. Toliyat, “Design comparison of NdFeB and ferrite radial flux surface permanent magnet coaxial magnetic gears,” *IEEE Trans. Ind. Appl*., vol. 54, no. 2, pp. 1254–1263, Mar./Apr. 2018.

[36] M. Johnson, M. C. Gardner, H. A. Toliyat, S. Englebretson, W. Ouyang, and C. Tschida, “Design, Construction, and Analysis of a Large-Scale Inner Stator Radial Flux Magnetically Geared Generator for Wave Energy Conversion,” *IEEE Trans. Ind. Appl*., vol. 54, no. 4, pp. 3305-3314, Jul./Aug. 2018.

[37] L. Jian, K. T. Chau and J. Z. Jiang, "A Magnetic-Geared Outer-Rotor Permanent-Magnet Brushless Machine for Wind Power Generation," *IEEE Trans. on Ind. Appl*., vol. 45, no. 3, pp. 954-962, May-june 2009.

[38] C. G. C. Neves, A. F. Flores Filho and D. G. Dorrel, "Design of a Pseudo Direct Drive for Wind Power Applications," in *Proc. Int. Conf. Asian Union Magn. Soc*., 2016, pp. 1-5.

[39] M. C. Gardner, M. Johnson and H. A. Toliyat, "Analysis of high gear ratio capabilities for single-stage, series multistage, and compound differential coaxial magnetic gears," *IEEE Trans. Energy Conv*., vol. 34, no. 2, pp. 665-672, June 2019.